Aharonov-Bohm oscillations in a quantum ring: Eccentricity and electric-field effects

A. Bruno-Alfonso*
Departamento de Matemática, Faculdade de Ciências, UNESP-Universidade Estadual Paulista, Avenida Luiz Edmundo Carrijo Coube sn, 17033-360, Bauru-São Paulo, Brazil

A. Latgé
Instituto de Física, UFF-Universidade Federal Fluminense, Avenida Litorânea sn, 24210-340, Niterói-RJ, Brazil
(Received 6 October 2004; published 15 March 2005)

The effects of an in-plane electric field and eccentricity on the electronic spectrum of a GaAs quantum ring in a perpendicular magnetic field are studied. The effective-mass equation is solved by two different methods: an adiabatic approximation and a diagonalization procedure after a conformal mapping. It is shown that the electric field and the eccentricity may suppress the Aharonov-Bohm oscillations of the lower energy levels. Simple expressions for the threshold energy and the number of flat energy bands are found. In the case of a thin and eccentric ring, the intensity of a critical field which compensates the main effects of eccentricity is determined. The energy spectra are found in qualitative agreement with previous experimental and theoretical works on anisotropic rings.

DOI: 10.1103/PhysRevB.71.125312 PACS number(s): 73.21.−b, 73.23.−b, 73.63.−b

I. INTRODUCTION

Quantum rings (QRs) are doubly connected mesoscopic systems where the ballistic motion of charge carriers may take place. Fortunately, many properties of QRs can be explained with single-electron theory.[1–3] In particular, the electrons in a perfectly circular ring threaded by a perpendicular magnetic field may have a well-defined projection of the angular momentum $L_z=\hbar l$ in the direction of the field. As a function of the threading magnetic flux ϕ, the energy of the state with $l=0$ gives an upward parabola with the vertex at $\phi=0$. Moreover, a horizontal shift of that curve in $-l\phi_0$, where $\phi_0=2\pi\hbar/e$, is obtained for other values of l. Hence, when the levels are indexed as energy increases, each of them performs periodic oscillations with period ϕ_0. Such oscillations are a result of a quantum-interference phenomenon which is known as the Aharonov-Bohm (AB) effect, and may be detected by transport measurements.[4] Optical experiments[5] has also detected the AB effect on a charged particle in a nanoscale QR.

Actually, the circular shape is an idealization of grown or fabricated solid-state rings, where imperfections of the structures often occur.[4] In order to study the manifestation of the AB effect in a less symmetric ring, a two-dimensional (2D) annular ellipse with smoothly varying width has been considered.[6] The asymmetry of the system was shown to produce the opening of gaps and the localization of some states in the wider regions, thus leading to the flattening of the corresponding energy levels. Also, the effect of the variable curvature of an elliptical QR of uniform width on the electron-energy spectrum in a magnetic field has been studied.[7] The expected AB oscillations were found, but energy gaps appeared due to the confinement of the electron in the regions with larger curvature. Moreover, the influence of the anisotropy of a semiconductor QR, as due to an applied electric field, on the AB oscillations and the optical spectrum has been analyzed.[8] It was found that in the presence of threading magnetic field, the electric field destroys the rotational invariance of the QR and suppresses the AB oscillations of the lower energy levels.

In the absence of the magnetic field, the electronic states in QRs subjected to an in-plane electric field[9] and including eccentricity effects[10] have been studied. We have calculated the electronic spectrum of eccentric rings by a combination of a conformal mapping with a matrix-diagonalization procedure.[10] In particular, we have shown that the ground-state polarization due to eccentricity may be compensated by an in-plane electric field. Also, 2D QRs of constant width and arbitrary centerline, where the effects of a varying curvature play a central role, have been considered.[11]

In this work, the conduction-electron states in GaAs quantum rings in the presence of a perpendicular magnetic field are calculated within the effective-mass approximation. The in-plane motion of the electron is restricted to the region between two nonconcentric circles. Attention is focused on the effects of the eccentricity and in-plane electric fields, which break the rotational symmetry of the ring.[8–10] The interplay between the electric field and the eccentricity is explained in terms of simple equations for each transversal mode, within an adiabatic approximation. In particular, we determine the number of flat energy levels and the spacing between them. For a comparison, we have calculated the same energy levels by adapting the method of Lavenère *et al.*,[10] to include the effects of the threading magnetic flux. The energy spectra are found in qualitative agreement with previous experimental and theoretical works on anisotropic rings.[4,8]

II. THEORETICAL FRAMEWORK

To study the electronic spectrum of a GaAs QR in crossed magnetic and electric fields, a parabolic-band scheme within the effective-mass approximation is used. Hence, the stationary envelope functions satisfy the equation

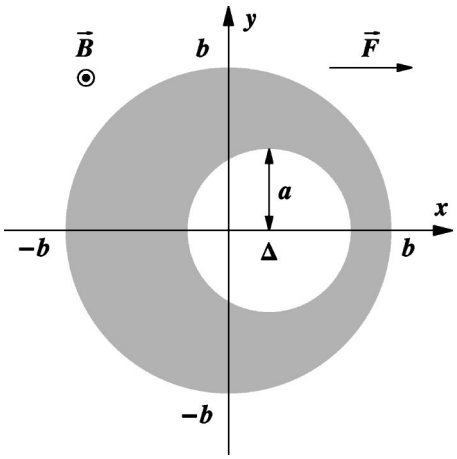

FIG. 1. Schematic view of a 2D ring under crossed electric $\vec{F}$ and magnetic $\vec{B}$ fields, with a and b being the internal and external radii, respectively. The shift Δ is the eccentricity.

$$\hat{H}_{3D}\psi_{3D}(\vec{r}) = E_{3D}\psi_{3D}(\vec{r}) \tag{1}$$

with

$$\hat{H}_{3D} = \frac{[-i\hbar\vec{\nabla} + e\vec{A}(\vec{r})]^2}{2m^*} + e\vec{F}\cdot\vec{r} + U_{3D}(\vec{r}), \tag{2}$$

where $U_{3D}(\vec{r})$ is the QR-confinement potential, $\vec{A}(\vec{r})$ is the vector potential of the magnetic field, and $\vec{F}$ is the electric-field intensity. Also, $-e$ is the electron charge and m^* is the effective mass ($m^*=0.067m_0$ for conduction electrons in GaAs, where m_0 is the electron mass).

The QR confinement is taken as $U_{3D}(\vec{r})=V(z)+U_{2D}(x,y)$, where $V(z)$ gives the vertical confinement and

$$U_{2D}(x,y) = \begin{cases} 0, \text{ if} (x-\Delta)^2 + y^2 \geqslant a^2 \text{ and } x^2+y^2 \leqslant b^2 \\ \infty, \text{ otherwise} \end{cases} \tag{3}$$

defines a doubly-connected region $\mathcal{R}$ in the xy plane. Actually, $\mathcal{R}$ is a ring with circular boundaries, where a (b) is the internal (external) radius and Δ is the eccentricity (with $|\Delta|<b-a$). The vector potential is chosen as $\vec{A}(\vec{r})=(\vec{B}\times\vec{r})/2$, where $\vec{B}=(0,0,B)$ is the magnetic field, and the electric field is taken as $\vec{F}=(F,0,0)$. The 2D ring $\mathcal{R}$ and the electromagnetic-field configuration are depicted in Fig. 1.

The envelope wave function may be written as $\psi_{3D}(\vec{r})=\chi(z)\psi_{2D}(x,y)$, where the in-plane wave function satisfies

$$\hat{H}_{2D}\psi_{2D}(x,y) = E_{2D}\psi_{2D}(x,y), \tag{4}$$

with

$$\hat{H}_{2D} = -\frac{\hbar^2}{2m^*}\nabla^2_{(x,y)} - \frac{ie\hbar B}{2m^*}\left(-y\frac{\partial}{\partial x} + x\frac{\partial}{\partial y}\right) + \frac{e^2B^2}{8m^*}(x^2+y^2) + eFx + U_{2D}(x,y), \tag{5}$$

being the in-plane Hamiltonian, which contains the effects of the eccentricity and the electric and magnetic fields. Moreover, the vertical wave function $\chi(z)$ satisfies

$$\left[-\frac{\hbar^2}{2m^*}\frac{d^2}{dz^2} + V(z)\right]\chi(z) = (E_{3D}-E_{2D})\chi(z). \tag{6}$$

The potential $V(z)$ is not specified here, but it is supposed to have a discrete set of low-energy levels.

Two different methods are used, in what follows, to solve Eq. (4): (i) an adiabatic approximation leading to a one-dimensional (1D) problem and (ii) a 2D approach involving a diagonalization procedure after a conformal mapping.[10] As those approaches involve coordinate transformations between the rectangular coordinates $(x_1,x_2)=(x,y)$ and a couple (q_1,q_2) of suitable curvilinear coordinates, it is convenient to establish a curvilinear version of Eq. (4).

The Laplace operator is transformed as[12,13]

$$\nabla^2_{(x,y)} = \frac{1}{J}\sum_{h=1}^{2}\frac{\partial}{\partial q_h}\left(J\sum_{j=1}^{2}G^{-1}_{jh}\frac{\partial}{\partial q_j}\right), \tag{7}$$

where $J=\det(M)$ is the Jacobian of the transformation, the Jacobian matrix satisfies

$$M_{hj} = \frac{\partial x_h}{\partial q_j}, \tag{8}$$

and $G=M^TM$ is the covariant metric tensor.[13] The curvilinear coordinates are chosen to guarantee that J is always positive. Also, the partial derivatives are transformed as

$$\frac{\partial}{\partial x_h} = \sum_{j=1}^{2}M^{-1}_{jh}\frac{\partial}{\partial q_j}. \tag{9}$$

The probability of finding the electron in $[x_1,x_1+dx_1]\times[x_2,x_2+dx_2]$ is given by $|\psi_{2D}(x_1,x_2)|^2dx_1dx_2 = |\eta(q_1,q_2)|^2dq_1dq_2$, with

$$\eta(q_1,q_2) = \psi_{2D}(x_1,x_2)\sqrt{J}, \tag{10}$$

and the orthonormality relations for $\eta(q_1,q_2)$ apply to $\psi_{2D}(x_1,x_2)$ as well.

The differential equation for $\eta(q_1,q_2)$ is

$$\hat{T}\eta(q_1,q_2) = E_{2D}\eta(q_1,q_2), \tag{11}$$

with

$$\hat{T} = -\frac{\hbar^2}{2m^*}\frac{1}{\sqrt{J}}\sum_{h=1}^{2}\frac{\partial}{\partial q_h}\left(J\sum_{j=1}^{2}G^{-1}_{jh}\frac{\partial}{\partial q_j}\frac{1}{\sqrt{J}}\right) - \frac{ie\hbar B}{2m^*}\sqrt{J}\sum_{h=1}^{2}(-1)^h x_{3-h}\left(\sum_{j=1}^{2}M^{-1}_{jh}\frac{\partial}{\partial q_j}\frac{1}{\sqrt{J}}\right) + \frac{e^2B^2}{8m^*}(x_1^2+x_2^2) + eFx_1 + U_{2D}(x_1,x_2), \tag{12}$$

where x_1 and x_2 are functions of q_1 and q_2. Equation (4) is then solved for $\psi_{2D}(x,y)$ in the region $\mathcal{R}$, where $U_{2D}=0$, with the Dirichlet boundary condition $\psi_{2D}(x,y)=0$.

III. THE ADIABATIC APPROXIMATION

If the ring $\mathcal{R}$ is thin enough, i.e., $b-a \ll b$, then it can be treated as a quasi-one-dimensional strip in the xy plane. Since the inner circle can be parameterized as $(x,y)=[\Delta+a\cos(\theta), a\sin(\theta)]$, with $-\pi \leqslant \theta \leqslant \pi$, and the outer circle is $(x,y)=[b\cos(\theta), b\sin(\theta)]$, a mean circle may be defined as $(x,y)=[\Delta/2+r\cos(\theta), r\sin(\theta)]$, with $r=(a+b)/2$ being the mean radius. The curvilinear coordinates $(q_1,q_2)=(u,\theta)$ are implicitly defined by

$$\begin{pmatrix} x \\ y \end{pmatrix} = \begin{bmatrix} (1/2-u)\Delta + (r+uw)\cos(\theta) \\ (r+uw)\sin(\theta) \end{bmatrix}, \tag{13}$$

with $w=b-a$ being the mean width, and $-1/2 \leqslant u \leqslant 1/2$. Hence, θ and u are the longitudinal and transversal coordinates, respectively. The Jacobian $J=(r+uw)[w-\Delta\cos(\theta)]$ of this transformation is a positive function for $u \in [-1/2, 1/2]$ and arbitrary θ.

After a lengthy but straightforward calculation, the operator $\hat{T}$ in Eq. (12) is obtained in terms of the small parameters $\Omega=w/r$ and $\xi=\Delta/w$. A first-order power expansion of $\hat{T}$ in terms of Ω and ξ is performed to obtain the Hermitian operator $\hat{T}_0$ (not shown, for the sake of brevity). The adiabatic approximation leads to a variational solution of

$$\hat{T}_0 \eta(u,\theta) = E_{2D}\eta(u,\theta), \tag{14}$$

where $\eta(u,\theta)=\sqrt{2}\sin(n\pi u+n\pi/2)\psi_{1D}(\theta)$, with $n=1,2,3,\ldots$ corresponding to different transversal modes. The longitudinal mode $\psi_{1D}(\theta)$ satisfies

$$\hat{H}_{1D}^{(n)}\psi_{1D}(\theta) = \left(E_{2D} - \frac{\hbar^2 n^2 \pi^2}{2m^* w^2}\right)\psi_{1D}(\theta), \tag{15}$$

with the cyclic boundary condition $\psi_{1D}(\theta+2\pi)=\psi_{1D}(\theta)$ for all values of θ. The Hamiltonian is

$$\begin{aligned} \hat{H}_{1D}^{(n)} &= 2\int_{-1/2}^{1/2} \sin(n\pi u + n\pi/2)\hat{T}_0 \sin(n\pi u + n\pi/2)du \\ &= \frac{\hbar^2}{2m^* r^2}\left[-\frac{d^2}{d\theta^2} - \frac{2i\phi}{\phi_0}\frac{d}{d\theta} + \frac{\phi^2}{\phi_0^2} + \frac{\alpha_n}{2}\cos(\theta)\right] \\ &\quad - \frac{\hbar^2}{8m^* r^2} + \frac{eF\Delta}{2}, \end{aligned} \tag{16}$$

where $\phi=\pi r^2 B$ is the magnetic flux over the mean circle, $\phi_0=2\pi\hbar/e$, and

$$\alpha_n = \frac{4m^* r^2}{\hbar^2}\left(eFr + \frac{\hbar^2 n^2 \pi^2 \Delta}{m^* w^3}\right) \tag{17}$$

is a parameter which measures the anisotropy of the system (due to the eccentricity and the applied electric field) for the nth transversal mode.

It is worth noting that the four terms in the parentheses of Eq. (16) contain most of the physics of the problem. In fact, the first three are responsible for the Aharonov-Bohm oscillations of the energy levels associated to the nth transversal mode, while the fourth term can suppress the oscillations of the energy levels below a certain threshold. Moreover, the last two terms in Eq. (16) lead to a shift of the energy levels that does not depend on the magnetic field.

The anisotropy parameter in Eq. (17) depends linearly on the electric-field intensity and the eccentricity. One may notice that the eccentricity effect is stronger for: (i) bigger and thinner rings (larger r and smaller w) and (ii) higher transversal modes (larger n), but it does not depend on the effective mass or the electric charge of the particle. On the other hand, the effect of the electric field is stronger for: (i) bigger rings and (ii) larger effective mass m^*, but it does not depend on the mean width w or the transversal-mode index n. Also, the electric-field term has opposite sign for a positive charge, i.e., for a hole. Moreover, α_n vanishes for the electric-field intensity

$$F_n = -\frac{\hbar^2 n^2 \pi^2 \Delta}{em^* w^3 r}. \tag{18}$$

It means that it is possible to repair the eccentric ring by applying an in-plane electric field, avoiding the suppression of the Aharonov-Bohm oscillations. However, the critical field-intensity F_n depends on the transversal-mode index n and the effective mass m^*, and has opposite signs for positive and negative charges. In this sense, it is not possible to mend the whole electronic spectrum of the eccentric ring.

The eigenfunctions of $\hat{H}_{1D}^{(n)}$ in Eq. (16) are

$$\begin{aligned} \psi_{1D}^{(j,n)}(\theta) = \frac{1}{\sqrt{2}}\exp\left(-i\frac{\phi}{\phi_0}\theta\right) \times \Bigg[& A_{j,n} C\left(4\lambda_{j,n}, \alpha_n, \frac{\theta}{2}\right) \\ & + B_{n,j} S\left(4\lambda_{j,n}, \alpha_n, \frac{\theta}{2}\right)\Bigg] \end{aligned} \tag{19}$$

with $j=1,2,3,\ldots$, and $C(a,q,z)$ and $S(a,q,z)$ being the even and odd (in the variable z) Mathieu functions, respectively, which are linearly independent solutions of the differential equation[14,15]

$$y''(z) + [a - 2q\cos(2z)]y(z) = 0. \tag{20}$$

Here, $C(a,q,z)$ $[S(a,q,z)]$ is the solution with the initial conditions $y(0)=1$ and $y'(0)=0$ $[y(0)=0$ and $y'(0)=1]$. According to the condition $\psi_{1D}(\theta+2\pi)=\psi_{1D}(\theta)$, the coefficients A_j and B_j satisfy

$$\begin{aligned} iA_{j,n}\sin\left(\frac{\pi\phi}{\phi_0}\right) C\left(4\lambda_{j,n}, \alpha_n, \frac{\pi}{2}\right) \\ = B_{j,n}\cos\left(\frac{\pi\phi}{\phi_0}\right) S\left(4\lambda_{j,n}, \alpha_n, \frac{\pi}{2}\right) \end{aligned} \tag{21}$$

and

$$\begin{aligned} A_{j,n}\cos\left(\frac{\pi\phi}{\phi_0}\right) C'\left(4\lambda_{j,n}, \alpha_n, \frac{\pi}{2}\right) \\ = iB_{j,n}\sin\left(\frac{\pi\phi}{\phi_0}\right) S'\left(4\lambda_{j,n}, \alpha_n, \frac{\pi}{2}\right), \end{aligned} \tag{22}$$

where $C'(a,q,z)=C_z(a,q,z)$ and $S'(a,q,z)=S_z(a,q,z)$. Hence, $\lambda_{j,n}=\lambda_j(\alpha_n,\phi)$ with $\lambda_j(\alpha,\phi)$ being the jth root of

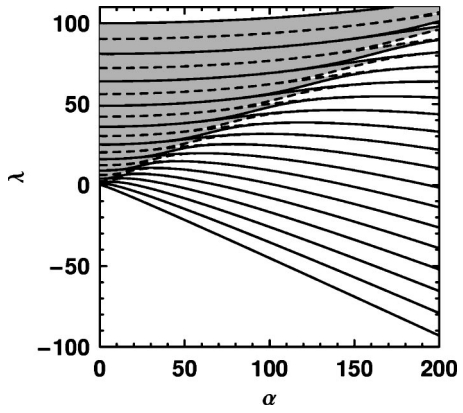

FIG. 2. Energy spectrum given by the roots $\lambda_j(\alpha,\phi)$ as a function of the anisotropy parameter α for the lower 20 bands ($j=1,\ldots,20$) and $0\leqslant\phi\leqslant\phi_0/2$. The solid (dashed) lines correspond to the magnetic flux $\phi=0$ ($\phi=\phi_0/2$) and the gray bands are for $0<\phi<\phi_0/2$.

$$\cos^2\left(\frac{\pi\phi}{\phi_0}\right)C'\left(4\lambda,\alpha,\frac{\pi}{2}\right)S\left(4\lambda,\alpha,\frac{\pi}{2}\right)= -\sin^2\left(\frac{\pi\phi}{\phi_0}\right)C\left(4\lambda,\alpha,\frac{\pi}{2}\right)S'\left(4\lambda,\alpha,\frac{\pi}{2}\right), \quad (23)$$

and the corresponding value of E_{2D} is

$$E_{2D}^{(j,n)}=\frac{\hbar^2n^2\pi^2}{2m^*w^2}+\frac{\hbar^2}{2m^*r^2}\left[\lambda_j(\alpha_n,\phi)-\frac{1}{4}\right]+\frac{eF\Delta}{2}. \quad (24)$$

From Eq. (23), it is straightforward to show that the spectrum is even $[\lambda_j(\alpha,-\phi)=\lambda_j(\alpha,\phi)]$ and periodic with period ϕ_0 $[\lambda_j(\alpha,\phi+\phi_0)=\lambda_j(\alpha,\phi)]$ as a function of the magnetic flux ϕ. Moreover, $\lambda_j(-\alpha,\phi)=\lambda_j(\alpha,\phi)$, due to symmetry. Then, one can limit the numerical calculations to the ranges $\alpha\geqslant 0$ and $0\leqslant\phi\leqslant\phi_0/2$, where $\lambda_j(\alpha,\phi)$ is a monotonic function
of ϕ. In a wider range of ϕ values, $\lambda_j(\alpha,\phi)$ exhibits AB oscillations as a function of ϕ with amplitude $\delta_j(\alpha)=|\lambda_j(\alpha,\phi_0/2)-\lambda_j(\alpha,0)|$. In particular, for $\alpha=0$ the bandwidth is given by $\delta_j(0)=(2j-1)/4$.

Figure 2 displays the eigenvalues $\lambda_j(\alpha,\phi)$ as a function of the anisotropy parameter α for $j=1,\ldots,20$ and $0\leqslant\phi\leqslant\phi_0/2$. The solid (dashed) lines correspond to $\phi=0$ ($\phi=\phi_0/2$) and the gray bands are for $0<\phi<\phi_0/2$. One can clearly distinguish between the bands above and below the line $\lambda=\alpha/2$, which corresponds to the maximum value of the potential $\alpha\cos(\theta)/2$ in Eq. (16). The higher bands are wide and very small gaps separate them. This means that such bands show strong Aharonov-Bohm oscillations. Instead, the lower bands are very narrow with large gaps between them.

Those flatbands occur because the asymmetry of the system leads to a confinement of the particle around $\theta=\pi+2k\pi$ ($\theta=2k\pi$) for $\alpha>0$ ($\alpha<0$), with k being an integer. In fact, the second-order Taylor expansion of the potential $\alpha\cos(\theta)/2$ in Eq. (16) around its minima is $|\alpha|$ $[(\theta-\theta_k)^2/4-1/2]$, where $\theta_k=\pi+2k\pi$ ($\theta_k=2k\pi$) for $\alpha>0$ ($\alpha<0$). Hence, for sufficiently large $|\alpha|$, the states with small index j correspond to a coupled set of linear oscillators.[16] The associated bands are almost flat and can be given in terms of an isolated oscillator as

$$\lambda_j(\alpha,\phi)\approx-\frac{|\alpha|}{2}+\left(j-\frac{1}{2}\right)\sqrt{|\alpha|}. \quad (25)$$

Since the line $\lambda=|\alpha|/2$ separates narrow and wide bands, Eq. (25) may be used to estimate the number of flatbands as

$$N_\alpha\approx\sqrt{|\alpha|}+\tfrac{1}{2}. \quad (26)$$

Of course, one should take the nearest positive integer to N_α. However, the Eq. (26) underestimates the value of N_α, since the spacing between consecutive bands decreases as j increases (see Fig. 2).

According to Eq. (24), the energy of the flatbands with small j and corresponding to the nth transversal mode can be given as

$$E_{2D}^{(j,n)}\approx\frac{\hbar^2n^2\pi^2}{2m^*w^2}-\frac{\hbar^2}{2m^*r^2}\left(\frac{|\alpha_n|}{2}+\frac{1}{4}\right)+\frac{eF\Delta}{2}+\frac{\hbar^2\sqrt{|\alpha_n|}}{2m^*r^2}\left(j-\frac{1}{2}\right), \quad (27)$$

which is a sequence of uniformly spaced levels separated by

$$s_n=\frac{\hbar^2\sqrt{|\alpha_n|}}{2m^*r^2}. \quad (28)$$

This is an important result which allows one to obtain the magnitude $|\alpha_n|$ of the anisotropy parameter in terms of the mean radius r, after the experimental determination of the level spacing. A further relation between the ring parameters is given by the threshold energy which separates narrow and wide bands. This energy is

$$E_{thr}^{(n)}=\frac{\hbar^2n^2\pi^2}{2m^*w^2}+\frac{\hbar^2}{2m^*r^2}\left(\frac{|\alpha_n|}{2}-\frac{1}{4}\right)+\frac{eF\Delta}{2}, \quad (29)$$

but the experimental error for $E_{thr}^{(n)}$ is of the order of s_n. Instead, the energy of the lower longitudinal mode $E_{2D}^{(1,n)}$ may be found more accurately. The latter establishes an important relation between the mean width w, the mean radius r, the eccentricity Δ and the electric-field intensity F [see Eq. (17)].

Figure 2 also shows that, below the threshold line $\lambda=\alpha/2$, the bandwidth $\delta_j(\alpha)$ decreases as the anisotropy parameter α increases. The actual width of the thinner bands, however, is not shown in the figure, because the thickness of the edge curves in the artwork is fixed. To better illustrate the evolution of the bandwidths, Fig. 3 displays the dependence of the rate $\delta_j(\alpha)/\delta_1(0)$ with the anisotropy α, for $j=1,\ldots,20$. One clearly sees that lower bands are thinner and that the bandwidths decrease exponentially for sufficiently large values of α. The number of flatbands, N_α, is also inferred from the figure. This is done by following a criterium in which a band is flat if it is thinner than a half of $\delta_1(0)$. With this idea in mind, N_α is the number of curves

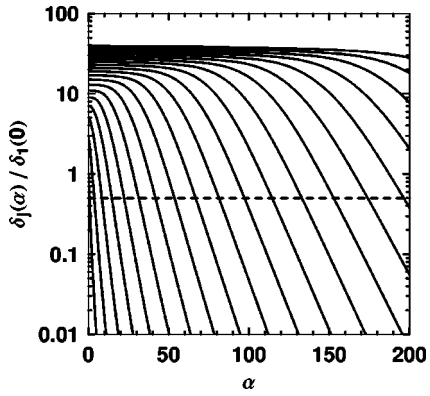

FIG. 3. The bandwidth $\delta_j(\alpha)$, in units of the width $\delta_1(0)$ of the first band in a concentric ring with electric field $F=0$, as a function of the anisotropy parameter α for $j=1,\ldots,20$. The band index j increases from the left-bottom to the right-top corner. The dashed line is for $\delta_j(\alpha)=\delta_1(0)/2$.

crossing the dashed line (depicted in the figure) at anisotropy parameters shorter than α. That number may be estimated by a simple fitting as

$$N_\alpha \approx -0.322 + 1.153\sqrt{|\alpha|}, \tag{30}$$

where the nearest positive integer to N_α should be taken. This number is relevant for the study of persistent currents in QRs, since the flatbands do not contribute to the current. Hence, the number of electrons in the ring should be greater than N_α for the AB oscillations to be detected in an equilibrium transport measurement.

It is worth noting that for a concentric GaAs QR with $r=400$ Å, $w\sim 20$ Å, and $F=10$ kV/cm, the anisotropy parameter of Eq. (17) is $\alpha\approx 225.1$ for all values of n. Hence, according to the Eq. (30), there are 17 flatbands for all the transversal modes. Moreover, the Eq. (28) gives the spacing between the lower bands $s_n\approx 5.33$ meV. These results are in good agreement with the work of Barticevic *et al.*[8]

IV. CONFORMAL MAPPING AND DIAGONALIZATION PROCEDURE

To simplify the solution of the Eq. (4), a conformal mapping which transforms the eccentric ring $\mathcal{R}$ in a concentric ring $\mathcal{R}'$ is used.[10] Considering the complex variables $\omega=x+iy$ and $\omega'=x'+iy'$, a suitable conformal mapping is

$$\omega' = f(\omega) = \frac{\omega - x_0}{1 - x_0\omega/b^2}, \tag{31}$$

where $x_0=b^2(1+L_1L_2-L_3)/(2\Delta)$, with $L_3=\sqrt{(1-L_1^2)(1-L_2^2)}$, $L_1=(\Delta-a)/b$, and $L_2=(\Delta+a)/b$. In fact, the function f maps $|\omega-\Delta|=a$ and $|\omega|=b$ onto $|\omega'-\Delta|=a'$ and $|\omega'|=b$, respectively. The external radius of the concentric ring $\mathcal{R}'$ is b and its internal radius is $a'=b^2(1-L_1L_2-L_3)/(2a)$.

The conformal transformation give the rectangular coordinates (x,y) in terms of the curvilinear coordinates $(q_1,q_2)=(x',y')$. The Jacobian of this mapping is $J=g^{-2}$, with

$$g = \frac{(1+x_0x'/b^2)^2 + x_0^2(y')^2/b^4}{(1-x_0^2/b^2)}, \tag{32}$$

and the Jacobian matrix is

$$M = \frac{1}{(1-x_0^2/b^2)g^2}\begin{pmatrix} \mu & \nu \\ -\nu & \mu \end{pmatrix}, \tag{33}$$

with $\mu=(1+x_0x'/b^2)^2-x_0^2(y')^2/b^4$ and $\nu=2x_0y'(1+x_0x'/b^2)/b^2$.

Equation (11) is solved in the region $\mathcal{R}'$ with the Dirichlet boundary condition $\eta(x',y')=0$, and

$$\hat{T} = \frac{\hbar^2}{2m^*}\left(\hat{N} + \frac{2\phi}{r^2\phi_0}\hat{L} + \frac{\phi^2}{r^4\phi_0^2}\hat{Q}\right) + eF\hat{X}, \tag{34}$$

with $\hat{N}=-g\nabla^2_{(x',y')}g$, $\hat{Q}=x^2+y^2$, $\hat{X}=x$, and

$$\hat{L} = \frac{i}{(1-x_0^2/b^2)}\left\{\frac{2x_0y'}{b^2} + y'\left(1+\frac{2x_0x'}{b^2}+\frac{x_0^2}{b^2}\right)\frac{\partial}{\partial x'} + -\left[(x'+x_0)\left(1+\frac{x_0x'}{b^2}\right) - \frac{x_0(y')^2}{b^2}\right]\frac{\partial}{\partial y'}\right\}. \tag{35}$$

For this purpose, the eigenfunctions are expressed as

$$\eta(x',y') = \sum_{l,m} c_{m,l}\,\eta^{(0)}_{m,l}(x',y'), \tag{36}$$

where l takes integer values, $m=1,2,3,\ldots$, and $\eta^{(0)}_{m,l}(x',y')$ is defined in our previous work.[10,17] For each of the electronic states, the energy E_{2D} in Eq. (11) and the corresponding coefficients $c_{m,l}$ are found by diagonalization of $\hat{T}$ in the orthonormal base $\eta^{(0)}_{m,l}(x',y')$. In the calculations, the base is truncated, and the accuracy of the results may be increased by taking a base with a larger number of elements.

V. FURTHER RESULTS AND DISCUSSION

Figure 4 displays the lower 2D energy levels as functions of the mean magnetic flux ϕ, for conduction electrons in GaAs QRs with $a=900$ Å, $b=1100$ Å, and different combinations of eccentricity Δ and electric-field intensity F. The solid lines are the eigenvalues obtained from Eq. (34) using $m=1,2,3$ and $l=-40,\ldots,40$, whereas the dashed lines are the results from Eq. (24) with $n=1$, following the adiabatic approximation. The field intensity $F=-84.2$ V/cm has been taken from the Eq. (18), for $\Delta=6$ Å and $n=1$. A good agreement between the 2D approach and the adiabatic approximation (solid and dashed lines) is apparent in the figure.

The energy spectrum corresponding to a concentric QR in the absence of electric fields is shown in Fig. 4(a), where the Aharonov-Bohm oscillations are clearly seen. Figure 4(b) shows the effect of applying the in-plane field $F=-84.2$ V/cm to the concentric QR. The oscillations of the lower levels are nearly suppressed,[8] since this field pushes the electron to the right-hand side of the ring. Following Eq. (17), the value of the anisotropy parameter is $\alpha_1\approx -29.61$. According to Eq. (30) the number of flat levels is 6, as can be seen in Fig. 4(b). Also, the results show that flat levels are

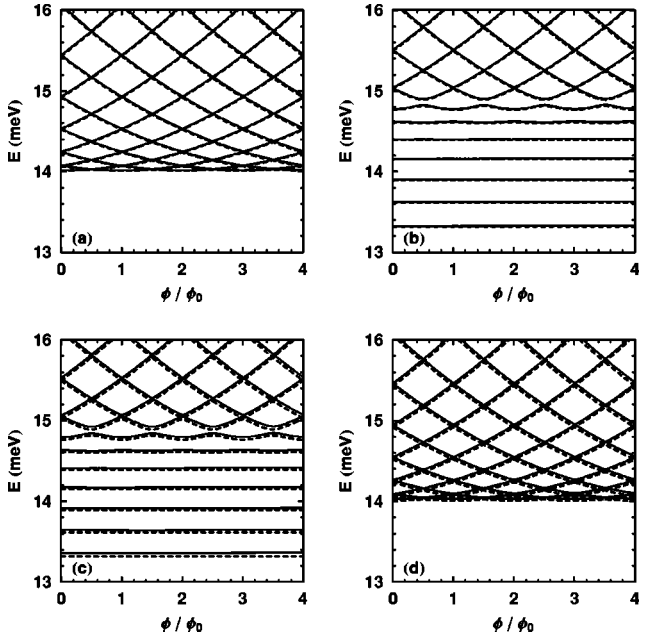

FIG. 4. The lower 2D energy levels as functions of the mean magnetic flux ϕ, for conduction electrons in GaAs QRs with $a=900$ Å, $b=1100$ Å, and (a) $\Delta=0$ Å and $F=0$ V/cm, (b) $\Delta=0$ Å and $F=-84.2$ V/cm, (c) $\Delta=6$ Å and $F=0$ V/cm, and (d) $\Delta=6$ Å and $F=-84.2$ V/cm. Solid (dashed) lines are the results of the 2D approach with the conformal mapping (the adiabatic approximation).

separated by $s_1\approx 0.31$ meV. A QR with eccentricity $\Delta=6$ Å is considered in the bottom panels of Fig. 4. Panel (c), where $F=0$ V/cm, shows that the eccentricity leads to the same effects as the in-plane electric field. In this case the localization of the electron occurs in the wider region,[6] and the picture resembles Fig. 4(b) since $\alpha_1\approx 29.61$. Instead, panel (d) for $F=-84.2$ V/cm is similar to Fig. 4(a), since the main effects of eccentricity and electric field are compensated, i.e., $\alpha_1\approx 0$.

Higher transversal electronic modes may also be apparent in experimental studies.[4] Figure 5 displays some high-energy levels for the system of Fig. 4(d). The solid lines are the eigenvalues of Eq. (34), with $m=1,2,3$ and $l=-40,\ldots,40$, whereas the dashed lines are given by the Eq. (24), with $n=1$ or $n=2$. The diamondlike structure with ~ 3 meV high pieces are associated to the first transversal mode, and clearly shows the AB oscillations. Moreover, the flat curves and the diamondlike structure with ~ 1 meV high pieces correspond to the $n=2$ transversal mode. For the latter states the anisotropy parameter is $\alpha_2\approx 88.82$, which leads to 11 flatbands. Also, the spacing between the lower flatbands is $s_2\approx 0.54$ meV. This shows that the in-plane electric field $F=-84.2$ V/cm, which recovers the oscillations of the $n=1$ level in Fig. 4(d), does not repair the $n=2$ states.

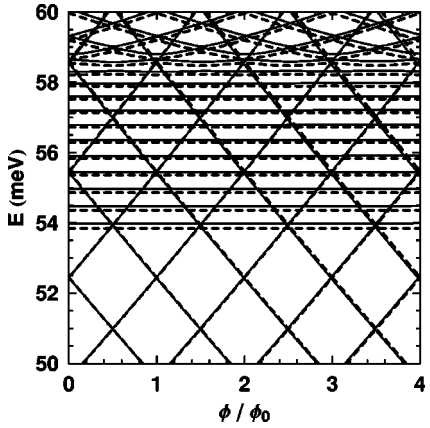

FIG. 5. Some 2D energy levels as functions of the mean magnetic flux ϕ, for conduction electrons in a GaAs QRs with $a=900$ Å, $b=1100$ Å, $\Delta=6$ Å, and $F=-84.2$ V/cm. Solid (dashed) lines are the results of the 2D approach with the conformal mapping (the adiabatic approximation).

VI. CONCLUSIONS

The conduction-electron states in GaAs quantum rings in the presence of a perpendicular magnetic field have been calculated within the effective-mass approximation, with special attention on the effects of in-plane electric fields and eccentricity. The calculation of the 2D states was performed by two methods: an adiabatic approximation and a conformal transformation combined with a diagonalization procedure.

The adiabatic approximation, which is suitable for sufficiently thin rings with small eccentricity leads to a 1D problem for each transversal mode. The main effects of the electric field and eccentricity are contained in the anisotropy parameter. We have shown that the eccentricity effect is stronger for bigger and thinner rings and higher transversal modes, but it does not depend on the effective mass or the electric charge of the particle. Moreover, the effect of the electric field is stronger for bigger rings and heavier particles and has an opposite sign for a positive charge and does not depend on the mean width of the ring or the transversal mode. Simple expressions have been derived for the threshold energy separating wide from narrow bands, the number of flat levels, the distance between the lower ones, and the energy of the ground level. Furthermore, the width of the flat energy bands, as functions of the threading magnetic flux, has been shown to decrease exponentially as the anisotropy parameter increases.

The 2D approach based on the combination of a suitable conformal mapping and a diagonalization procedure is more complete, since it includes the coupling between different transversal modes and remains valid for a wider range of ring dimensions and eccentricity values. A good agreement between the two approaches was obtained for thin rings with small eccentricity. As the electric field and the eccentricity may affect the electronic spectrum of GaAs quantum rings in the presence on a perpendicular magnetic field, we expect this work to be useful in magnetization, transport, and optical studies of such systems.

ACKNOWLEDGMENTS

The authors are grateful to the Brazilian Agencies FAPESP, FAPERJ, and CNPq for financial support.

*Electronic address: alexys@fc.unesp.br

[1] S. Viefers, P. Koskinen, P. S. Deo, and M. Manninen, Physica E (Amsterdam) **21**, 1 (2004).
[2] A. Bruno-Alfonso and A. Latgé, Phys. Rev. B **61**, 15 887 (2000).
[3] Z. Barticevic, M. Pacheco, and A. Latgé, Phys. Rev. B **62**, 6963 (2000).
[4] A. Fuhrer, S. Lüscher, T. Ihn, T. Heinzel, K. Ensslin, W. Wegscheider, and M. Bichler, Nature (London) **413**, 822 (2001).
[5] M. Bayer, M. Korkusinski, P. Hawrylak, T. Gutbrod, M. Michel, and A. Forchel, Phys. Rev. Lett. **90**, 186801 (2003).
[6] D. Berman, O. Entin-Wohlman, and M. Ya. Azbel, Phys. Rev. B **42**, 9299 (1990).
[7] L. I. Magarill, D. A. Romanov, and A. V. Chaplik, JETP **83**, 361 (1996).
[8] Z. Barticevic, G. Fuster, and M. Pacheco, Phys. Rev. B **65**, 193307 (2002).
[9] J. M. Llorens, C. Trallero-Giner, A. Garcia-Cristobal, and A. Cantarero, Phys. Rev. B **64**, 035309 (2001).
[10] L. A. Lavenère-Wanderley, A. Bruno-Alfonso, and A. Latgé, J. Phys.: Condens. Matter **14**, 259 (2002).
[11] D. Gridin, A. T. I. Adamou, and R. V. Craster, Phys. Rev. B **69**, 155317 (2004).
[12] I. J. Clark and A. J. Bracken, J. Phys. A **29**, 339 (1996).
[13] L. I. Magarill and M. V. Étnin, J. Exp. Theor. Phys. **96**, 766 (2003).
[14] L. Chaos-Cador and E. Ley-Koo, Rev. Mex. Fis. **48**, 67 (2002).
[15] J. C. Gutiérrez-Vega, R. M. Rodríguez-Dagnino, M. A. Meneses-Nava, and S. Chávez-Cerda, Am. J. Phys. **71**, 233 (2003).
[16] J. C. Slater, Phys. Rev. **87**, 807 (1952).
[17] There is a mistype in the second term of Eq. (21) in Ref. 10. The authors wrote the number 6 instead of the correct value 2.